Experimental Thermal and Fluid Science 121 (2021) 110291

Contents lists available at ScienceDirect

Experimental Thermal and Fluid Science

journal homepage: www.elsevier.com/locate/etfs

Effective use of the streamwise waviness in the control of turbulent separation

Artur Dróżdż, Paweł Niegodajew, Mathias Romańczyk, Vasyl Sokolenko, Witold Elsner

Czestochowa University of Technology, Institute of Thermal Machinery, al. Armii Krajowej 21, 42-200 Czestochowa, Poland

ARTICLE INFO

Keywords:
Turbulent boundary layer
Adverse pressure gradient
Flow control
Turbulent separation
Amplitude modulation
Convection velocity

ABSTRACT

It is commonly known that for a sufficiently high Reynolds number, for flow over a rough surface and other previously examined wall topologies, turbulent boundary layer separation generally occurs earlier, and the separation bubble is noticeably larger due to a greater momentum deficit caused by wall irregularities. The recently discovered amplitude modulation effect has provided an improved understanding of the momentum transport that occurs from the outer to the inner part of the boundary layer and its subsequent effect on skin friction. At sufficiently large Reynolds numbers, large-scale motion first causes an increase and then decrease in the flow velocity near the wall. This results in an increased net convection velocity of small structures in the streamwise direction, and consequently an increase in wall shear stress. In this work, we demonstrate that a wavy wall, with a streamwise waviness with carefully selected amplitude and period, can effectively enhance the amplitude modulation effect and ensure an increase in the wall shear stress, thereby postponing turbulent separation. The experimental results are presented in normalized general form using suitable flow scaling. The research goal is to find values of the amplitude, period, and length (always with the total number of periods) of the wavy wall for which the highest rise in skin friction is gained at a fixed point downstream of the wavy wall. The most effective wavy wall geometry investigated ensured a 13% increase in skin friction (relative to the value at zero-pressure-gradient inlet flow) at the location where flow separation occurred on an unmodified surface (i.e. on a flat plate).

1. Introduction

When a turbulent boundary layer (TBL) is exposed to an adverse pressure gradient (APG), separation is expected to occur at a certain point, which is difficult to predict. Boundary layer detachment from the bounding surface is accompanied by a rotational flow region just behind the separation point. When turbulent separation occurs on the upper surface of an airplane wing, a rapid decrease in lift force is observed. This problem also affects other applied systems, such as diffusers or mobile vehicles, where TBL detachment is responsible for substantial energy losses. In turn, this issue has attracted widespread attention and has stimulated considerable efforts to search for techniques that can postpone turbulent separation.

The development of TBL in APG is accompanied by a decrease in wall shear stress $\tau_w = \mu \mathrm{d}U/\mathrm{d}y$ (where μ is the dynamic viscosity, U is the streamwise velocity component, and y is the wall-normal coordinate) in the streamwise direction. Separation usually takes place when τ_w reaches zero [1]. Hence, an effective method to postpone separation should either increase τ_w locally (when separation is expected to occur) or reduce its decreasing rate within the entire APG section.

The available literature offers a variety of different approaches for flow separation control, which are generally classified as either active or passive. The former involve a number of different methods, such as dilution of polymer additives in flowing liquids [2,3], gas injectors [4,5], uniform blowing and suction [6], heating and cooling processes [7,8], moving wall systems [9,10], or exposing the flow to an electromagnetic field [11]. These methods, although usually effective, require considerable energy input, which leads to higher energy consumption and a reduction in total efficiency. Consequently, widespread attention has been paid to passive methods, as they do not require an external energy source.

Previous works provide many passive flow control solutions, from very fundamental studies of rough surfaces and simple geometries, to more advanced shapes and mechanical solutions. In some cases, their selection was inspired by nature, such as herringbone riblets [12] or topographies that mimic shark or dolphin skins [13,14]. Many have focused on drag reduction [15] rather than on flow separation control; however, they are still worth mentioning. The most fundamental case and the most widely investigated is the rough surface as in fact any

E-mail address: arturdr@imc.pcz.czest.pl (A. Dróżdż).

https://doi.org/10.1016/j.expthermflusci.2020.110291
Received 18 June 2020; Received in revised form 8 October 2020; Accepted 1 November 2020
Available online 6 November 2020

Nomenclature

A	amplitude of waviness
A_{in}	amplitude of the first waviness crests
A^+	fixed wave amplitude in viscous units
C_p	pressure coefficient
E	wavelet energy spectrum
H	shape factor
L	total corrugation length
l^+	non-dimensional wire length
n	number of periods
P_e	external pressure
Re_b	bulk velocity Reynolds number
Re_c	chord Reynolds number
Re_x	developing distance Reynolds number
Re_τ	friction velocity Reynolds number
Re_θ	momentum thickness Reynolds number
U	streamwise velocity component
U_c	convection velocity
U_e	boundary layer edge velocity
U^+	non-dimensional velocity
u_τ	friction velocity
x	distance in the measuring section
y	wall normal coordinate
y^+	non-dimensional wall distance

Greak symbols

β	Clauser-Rotta pressure gradient parameter
δ	boundary layer thickness
δ_{99}	boundary layer thickness (99% of the edge velocity U_e)
$\delta_{99,in}$	boundary layer thickness at the inlet plate
δ^*	displacement thickness
θ	momentum thickness
λ	wavelength
μ	dynamic viscosity
ν	kinematic viscosity
ρ	density
τ_w	wall shear stress

Abbreviations

APG	adverse pressure gradient
FPG	favourable pressure gradient
LSM	large-scale motion
OFI	oil-film interferometry
TBL	turbulent boundary layer
ZPG	zero pressure gradient
CCCM	corrected Clauser-chart method

considered surface is rough relative to the scale of the viscous length, and this scale decreases upon increasing the Reynolds number. It has been recognised in earlier literature [16,17] that the effect of rough surfaces on TBL leads to a shift in the log-linear region towards the wall, relative to a smooth wall, without changing its slope. This feature is commonly known as the roughness function. This shift is due to enhanced energy transfer from turbulent fields [18], and this effect is more pronounced when increasing the Reynolds number [19,20]. In APG flows, separation is postponed when the roughness is used for laminar or transitional flow regimes. However, at high Reynolds numbers, detachment occurs earlier, and the separation bubble is noticeably larger on rough surfaces due to the momentum deficit caused by wall irregularities [21–23]. A combination of surface roughness and APG enhances the Reynolds stress (in particular, the wall-normal and Reynolds shear stress) and turbulence production beyond the roughness sublayer [24]. The effect of roughness on TBL can be well-controlled by applying two-dimensional ribs [25,26] or grooves [27] because their pitch-to-height ratio can be freely changed. Other, more complex regular textures, have also been designed to reduce drag, such as sinusoidal riblets [28,29] or herringbone riblets [12]. Surface roughness is frequently used as a tripping device to help acquire well-behaved flow conditions [30,31], in particular in short wind tunnels, where the development of TBL at high Reynolds numbers is usually required [32]. It is interesting to note that rough wing profiles have a higher lift-to-drag ratio than smooth ones for chord Reynolds numbers, $Re_c < 10^5$ (where c is the chord of the wing); however, above this value, the effect is opposite, and the use of a rough surface does not provide additional benefits [33].

Regarding passive methods for postponing flow separation, a number of diverse attempts have been proposed, and some are widely applied in practice. Installing a microcylinder in front of the leading edge of an airfoil leads to an increased velocity on the upper surface and effectively suppresses separation on the blade surface [34,35]. Slotted airfoils (at a sufficiently high angle of attack) can ensure a higher lift force coefficient compared with their solid versions by providing kinetic energy to the suction side [36,37]. Attaching a Gurney flap (a short flat plate) to the trailing edge perpendicularly to the chord line on the pressure side of a wing can increase the lift coefficient at both subsonic and transonic speeds [38]. Serration of the leading edge of the blade is another interesting approach that can be used to control the flow separation and to improve the lift force at low Reynolds numbers [39]. Vortex generators, i.e. rectangular or triangular plates (also known as delta wings), arrayed periodically along the spanwise direction of a wing were effective at enhancing the momentum and energy transport nearest the wall, which postponed turbulent separation [40].

All the above-mentioned methods were more or less discussed in the well-known review paper of Gad-el-Hak [1]. A more recent survey on passive flow control techniques of Zhu and co-workers [41] showed that worldwide research effort is mostly focused on improving already-known methods rather than on searching for new solutions.

The development of new flow control methods is not possible without detailed insight into the physical processes taking place nearest the wall. The recent progress in both measuring and computational techniques has allowed the acquisition of valuable data, which provides a better understanding of the phenomena occurring in TBL at high Reynolds numbers. The hot wire rake measurements of Hutchins and Marusic [42] confirmed the presence of $>20\delta$ in length superstructures, also generally known as large-scale motion (LSM), in the log-region of TBL, which carry a substantial portion of the Reynolds shear stress. These scales become larger with increasing Reynolds number, and a single superstructure is statistically larger than a near-wall structure by a factor of at least $6Re_\tau/1000$. The authors also showed that these very large structures affect the small ones residing in the near-wall region. This issue became an object of even more detailed research summarised in another work by the same authors [43], in which they decomposed fluctuating velocity signals to search for potential interactions between large- and small-scale components of the signal. It was found that when the large-scale component of the velocity fluctuation took a negative value, the amplitude of the small-scale component was noticeably reduced. The opposite effect was observed when the large-scale component was positive – the amplitude of the small-scale velocity fluctuations was substantially increased. Today, this effect is commonly known as the large-scale amplitude modulation, and as shown in Ref. [44], it becomes progressively stronger with increasing Reynolds number and when a flow encounters APG conditions [45]. It means that this effect is important to practical flow scenarios that often occur at

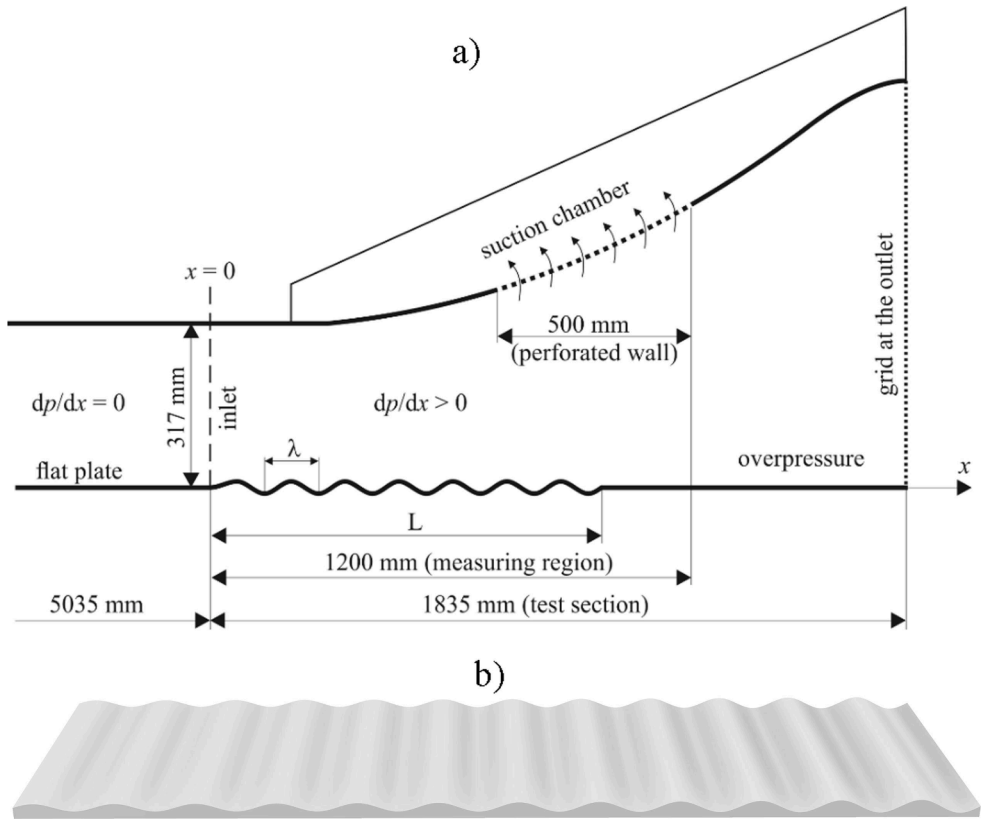

Fig. 1. Test section geometry (a), actual wavy-wall geometry (b). Flow from left to right.

high Reynolds numbers.

Recently, the effect of amplitude modulation has also been examined for flow over rough surfaces. It was confirmed that there exists the outer-layer similarity between smooth and rough walls [46,47]. Pathikonda and Christensen [48] confirmed that the near-wall small-scale respond to the outer large-scales, regardless of how they were generated, i.e. either via the turbulence production cycle or by vortex shedding behind roughness elements. Anderson [49] demonstrated that in the case of a rough wall, amplitude modulation was present in the roughness sub-layer, and the interactions between LSM and small-scales were stronger than in the smooth-wall flow.

Baars et al. [50] found that the amplitude modulation process can influence the convection velocity according to the quasi-steady quasi-homogeneous description of scale interactions of Zhang and Cherny-shenko [51]; however, the research was limited to ZPG TBL only. These findings were supported by Dróżdż [52] who investigated the effect of favourable pressure gradient (FPG) and APG on convection velocity. The author found that the LSMs were less active in FPG, and due to the absence of high- and low-speed regions, the production of vortices was random. In APG, the LSMs were noticeably more active and may generate small-scales with much higher convection velocities. Later on, Dróżdż and Elsner [53] investigated the influence of amplitude modulation on the convection velocity of the small-scales in APG flow. It was discovered that the convection velocity of the small-scales was higher with respect to the mean flow up to the upper bound of the inner region, while its highest change was reported in the buffer layer (reaching a value twice as high as the mean velocity at a high pressure gradient) [54]. An increased convection velocity is induced by LSM as it forces the production of the near-wall turbulence in the so-called high-speed regions. Under such specific conditions, where both convection and energy of small-scales are increased, a local enhancement of the sweep events occurs [53]. This local increase in sweep events cannot be balanced by locally-enhanced ejection events in the low-speed regions due to decreased convection and lower production of the near-wall turbulence (in that region). This results in higher momentum transfer to the wall and finally a rise in skin friction. This indicates that the quasi-steady and quasi-homogeneous description of scale interactions is no longer valid, especially in APG flows, where the skin friction is enhanced due to the nonlinear effect of the amplitude modulation. This mechanism is additionally supported by the research of Agostini and Leschziner [55] who confirmed a substantial contribution of the amplitude modulation to the skin friction caused by indirect effect (via shear-strain) of LSM on small-scales in the upper part of the buffer layer, even for ZPG flows.

Taking into account that the wall shear stress depends on the modulated convection velocity of the small-scales in the inner region, to increase the skin friction and ensure postponement of turbulent separation in APG, one needs to design a wall topology that can enhance the amplitude modulation effect. Especially promising may be the use of a wavy surface in the flow direction because such a corrugation type (with a carefully selected amplitude and period) does not affect the flow in the outer region [56,57]; hence, it should also not affect the superstructures residing in the log-region. The study of flow in channels with a wavy surface is challenging due to a multitude of flow parameters that should be considered when changing the amplitude-to-wavelength (A/λ) ratio [58]. In turn, the opposite effects of the wavy surface on the wall shear stress can be found in previous studies. In some works, the authors recorded a decrease in skin friction when surface undulations were introduced [59,60]. Direct numerical simulations of turbulent flow above a periodically-deformed film by Koyama et al. [61] showed that it is possible to enhance the skin friction when the period of the wall deformation is longer than the ratio of the wavelength of deformation to the fluid velocity in the buffer region. The authors explained that the effect was due to enhanced mixing in the wall-normal direction and changes in the sweep events caused by the deformation. Numerical simulations of Yoon et al. [62] for turbulent flow in a stationary wavy

Table 1
Wavy wall geometries.

Case	A_{in} [m]	λ [m]	A_{in}/λ	L [m]	$L/\delta_{99,in}$	A^+	$\lambda/\delta_{99,in}$	$A^+/(\lambda/\delta_{99,in})$	n	τ_w [Pa]
0			flat plate (reference case)							0.219
1	0.0025	0.100	0.0251	0.8	10.3	128	1.28	99.8	8	0.265
2	0.0045	0.100	0.0443	0.8	10.3	226	1.28	176	8	0.249
3	0.0054	0.100	0.0534	0.8	10.3	272	1.28	212	8	0.196
4	0.0034	0.067	0.05	0.8	10.3	170	0.854	198	12	0.206
5	0.0034	0.133	0.025	0.8	10.3	170	1.71	99.5	6	0.291
6	0.0034	0.067	0.0501	0.666	8.54	170	0.854	198	10	0.284
7	0.0025	0.100	0.0251	0.7	8.97	128	1.28	101	7	0.233
8	0.0025	0.100	0.0251	0.9	11.5	128	1.28	97.5	9	0.227
9	0.0034	0.133	0.025	0.666	8.54	170	1.71	99.5	5	0.290

channel showed that $A/\lambda = 0.03$ (at a bulk Reynolds number of 6760), for which the maximum increase in mean wall shear stress was obtained. Khan and Jayaraman [63] explained that increased drag was caused by enhanced turbulent stresses due to increased production of vertical velocity variance caused by the surface waviness. Segunda et al. [64] observed that the overall normal Reynolds stress profile increased with an increasing number of wave periods. The most substantial difference between profiles was observed between the first and second waves, and no further changes in profiles were visible when the number of waves was >8 (for $A/\lambda = 0.1$). Similar observations were noted by Hamed et al. [65]; however, a substantial increase in the overall Reynolds stress profiles was obtained over the first three wavelengths only ($A/\lambda = 0.05$).

One should note that all the mentioned flow cases were investigated under zero-pressure gradient (ZPG) conditions; hence, flow separation was observed only locally, i.e. in troughs. It is of interest to determine whether the effect of increased skin friction can be achieved in APG using a wavy surface and, more importantly, how it may affect turbulent separation.

In the paper of Dróżdż et al. [66], the authors investigated the effect of waviness for A/λ ranging from 0.025 to 0.08 had on the skin friction measured by oil film interferometry 240 mm downstream of the corrugated surface under APG conditions. They compared the results with a reference case in which TBL was developed on a flat plate. The experiment was performed for the Reynolds number based on momentum thickness Re_θ = 10,150 which corresponds to the Reynolds number based on a friction velocity Re_τ equal to 3300. A huge growth of 13% (relative to the inlet condition) in the skin friction was observed for $A/\lambda = 0.067$, which was accompanied by a significant increase in the mean velocity in the inner region ($<0.3\delta$). This was most probably caused by an enhanced amplitude modulation effect by surface waviness.

In this study, we would like to extend our preliminary research by exploring the possibility of using surface undulations to enhance the convection velocity and thereby strengthen the amplitude modulation effect. We expect that it will allow the control of turbulence detachment at high Reynolds numbers, which is not possible with rough surfaces. Additionally, this work investigates the effect of the total corrugation length L to find the pressure gradient limit for which surface undulations can be effectively applied. The key goal of the research is to examine the effect of wall corrugation on the skin friction – it is expected to provide a comparable increase in τ_w for Re_θ = 14,600 relative to the results obtained in Ref. [66]. It is worth noting that the research undertaken in this work has a pioneering character, as such an attempt aimed at postponing separation at high Reynolds number using wall topology modification has not been undertaken in the past.

2. Methods

2.1. Wind tunnel

The experiment was performed in an open-circuit wind tunnel. Fig. 1 illustrates the 1835 mm-long and 250 mm-wide APG diffuser-shape test section with the location of the wavy wall. To obtain the TBL close to separation at the bottom flat plate, the suction of the flow at a distance of 500 mm in the streamwise direction prior to the end of the measuring section was applied through the perforated (with 0.5 mm holes – giving 10% perforation in total) curved upper wall. To obtain a high Reynolds number flow, a 5 m-long ZPG section was applied prior to the test section. This allowed achieving a Reynolds number based on the developing distance $Re_x = 10^7$ (which is characteristic for a number of practical cases – for instance, flow over an airfoil) under an inlet velocity of 24 m/s, which is far beyond the limitation of flow control methods adopting turbulizers ($Re_x = 10^5$) [33]. To trip the boundary layer, coarse-grained sandpaper was mounted from 212 to 250 mm after the leading edge of the flat plate. To avoid extensive build-up of the side boundary layers, two pairs of suction gaps were mounted on the sidewalls of the inlet rectangular channel prior to the test section. Additionally, triangular inserts were mounted in the corners all along the inlet section to minimise the effect of secondary vortices. More technical details about the experimental stand can be found in previous work [67].

The wavy surface used in the experiment was characterised by the amplitude A, period λ, and length L (always with a total number of periods n). All these parameters were changed during the experiment to examine their effect on skin friction. To obtain effective wall undulation, the amplitude of each wavy wall was increasingly grown in the streamwise direction in such a way to have a fixed wave amplitude in viscous units $A^+ = Au_\tau/\nu$ which is independent of x. Each wavy wall was always mounted just after the inlet plane, i.e. at $x = 10$ mm. The details about the normalised parameters of the wavy walls investigated are collected in Table 1, where A_{in} is the amplitude of the first waviness crests and $\delta_{99,in}$ is the boundary layer thickness at the inlet plate, (i.e. at $x = 0$), which for all the cases was equal to $\delta_{99,in} = 77.8$ mm. The wavy wall was manufactured from high-density polyurethane to ensure a hydraulic smoothness of the surface just after mechanical processing. The actual geometry of the selected wavy wall is shown in Fig. 1b.

2.2. Measuring technique

Hot-wire anemometry (HWA) using a Streamline-Pro DANTEC device was used to conduct the velocity and its fluctuation measurements. The probe with a wire length of 0.4 mm and a diameter of 3 μm was used. The selection of such wire dimensions ensured maintaining a non-dimensional wire length ($l^+ = lu_\tau/\nu$, where u_τ is the friction velocity, and ν is the kinematic viscosity) below 20, in order to avoid filtration of small-scales, as advised in previous work [68]. Data acquisition was performed with a sampling frequency of 50 kHz and with a sampling time of 90 s. Variations in temperature when measuring a single velocity profile were not larger than ± 0.2 K. When the temperature in the wind tunnel was far from the calibration temperature, temperature-based voltage correction was automatically performed. During the whole experiment, the free-stream velocity and static pressure at the inlet plane ($x = 0$) and the pressure at the suction chamber were monitored with uncertainties of 1%, 10%, and 2.5%.

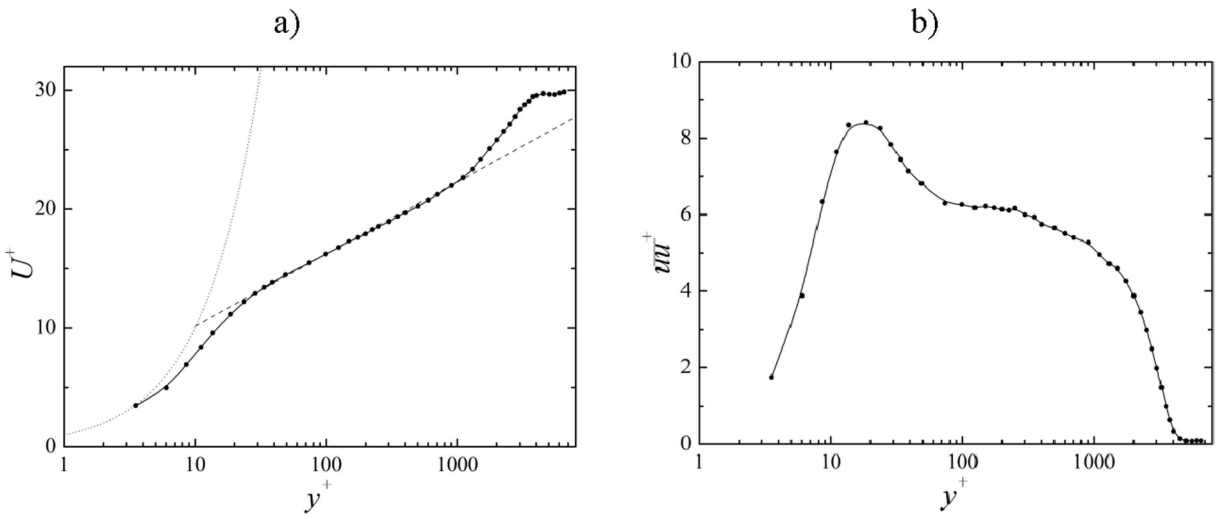

Fig. 2. Mean velocity (a) and turbulence intensity (b) profiles presented in viscous scale at $x = 0$. The dashed line represents the logarithmic law (with $\kappa = 0.38$ and $B = 4.1$) while the dotted line represents $y^+ = U^+$.

3. Research plan

The experimental procedure consisted of the following steps. Firstly, for fixed-flow conditions, i.e. for the Reynolds number based on momentum thickness $Re_\theta = 14{,}600$ (which is equivalent to the Reynolds number based on friction velocity $Re_\tau = 4000$) the measurements of the velocity and turbulence intensity profiles were performed at several distances (x = 0, 900, 1000, 1100, and 1200 mm) within the measuring section without a wavy surface mounted in the test section (to obtain reference data). Next, the wavy surface was installed in the test section, and then the measurements of the velocity and turbulence intensity profiles were performed at a fixed distance $x = 1000$ mm (always located at the flat plate behind the corrugation). With the measured profiles, one could estimate the friction velocities according to the procedure proposed by Niegodajew et al. [69] whose validity for the region behind the corrugation has been confirmed – see the appendix. For a wavy wall ensuring the highest growth in wall shear stress at $x = 1000$ mm, additional velocity and turbulence intensity measurements were performed at $x = 900$, 1100, and 1200 mm to provide information about the downstream effect. Note, that each time when a wavy wall was replaced with another one, the suction flux was adjusted to ensure the same distribution of the pressure gradient. This is necessary because when the skin friction increases, the boundary layer thickness decreases, and more suction is needed to obtain the same conditions in the free stream.

4. Inlet and pressure gradient conditions

The experiment was performed for relatively high Reynolds numbers based on the momentum thickness $Re_\theta = 14{,}700$. Fig. 2 shows the profiles of the mean velocity (a) and the streamwise Reynolds stresses (b) in the viscous units at the inlet plane of the measuring section ($x = 0$ mm), measured for the reference case (with a flat bottom wall). As is known, the logarithmic region of TBL begins with $y^+ = 150$ [70]. Hence, as the amplitude of the surface undulations analysed in the present experiment ranged from $A^+ = 125$ to $A^+ = 272$, the waviness crests for some cases reached the overlapping region. Note that the wavy wall amplitude should be much smaller than the boundary layer thickness δ_{99} (where the subscript "99" corresponds to the velocity value at the wall-normal location where 99% of the velocity at the edge U_e is reached). Fig. 2b indicates that the maximum velocity fluctuation at $y^+ \approx 15$ was slightly attenuated compared with the ones shown in Ref. [71]. This is the effect of both a relatively high Reynolds number and lower spatial resolution

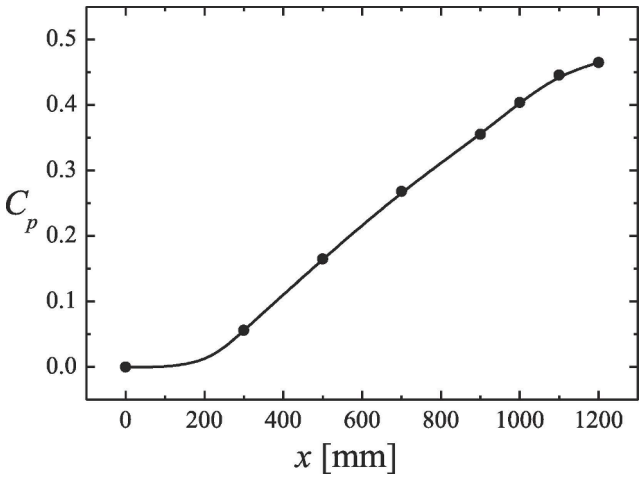

Fig. 3. Axial development of pressure coefficient.

investigated here.

Fig. 3 presents the axial distribution (within the entire measuring region – from $x = 0$ to 1200 mm) of the pressure coefficient $C_p = 1 - (U/U_e)^2$, which increases from 0 to 0.46 in the downstream direction. The distributions of other important TBL parameters, such as boundary layer thickness, Clauser-Rotta pressure gradient parameter β (defined as: $\beta = \frac{\delta^*}{\tau_w}\frac{dP_e}{dx}$, where δ^* is the displacement thickness, and τ_w is the wall shear stress) and shape factor $H = \delta^*/\theta$ are shown further in the paper in Fig. 8 (as they are confronted with the results obtained using the wavy surface). Uncertainties of the measurement of the mean velocity U, δ_{99}, and H, were estimated to be 1.0%, 3%, and 1.5%, respectively. The uncertainty of the probe wire location in the normal direction was $\Delta y = \pm 0.02$ mm. According to Ref. [69], the uncertainty of the skin friction estimation approach was ~ 5% for profiles characterised by $H < 2.0$ and up to ~ 11% for $H > 2.0$. The shape factor was corrected for the profiles near the separation by excluding from the integration process velocity values below 1.5 m/s and parts of the profile with a significant overshoot above $U^+ = y^+$ distribution. Overestimated velocity values may be produced due to the directional insensitivity of the hot-wire probe and/or due to the wall-proximity effect [72]. Both effects, however, are of minor importance as the skin frictions (for each case in Table 1) were estimated based on the outer part of turbulence

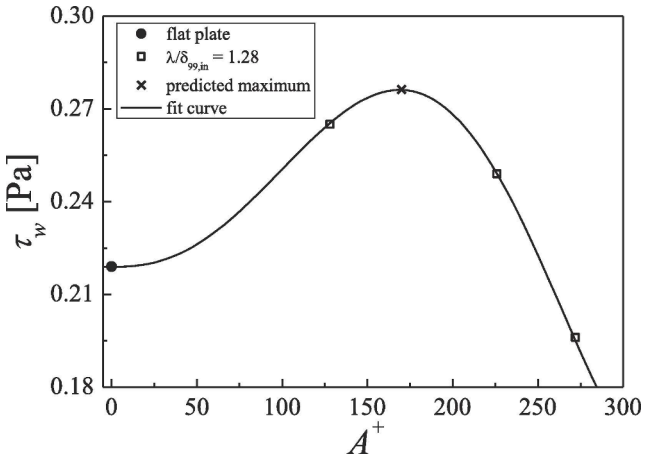

Fig. 4. Effect of wave amplitude on the wall shear stress in the measuring section at $x = 1000$ mm.

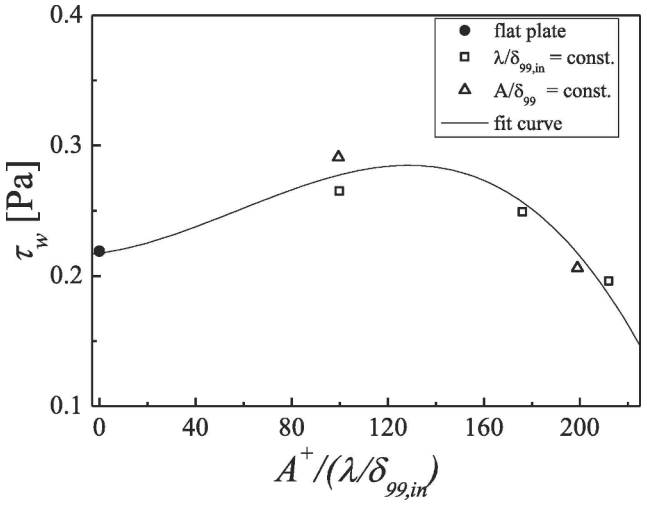

Fig. 5. Effect of both wave amplitude and period on the wall shear stress in the measuring section at $x = 1000$ mm.

intensity and mean velocity profiles according to [69]. It should be noted that the wind tunnel configuration ensured maintaining so-called well-behaved ZPG flow conditions during the experiment, i.e. values of the friction coefficient and shape factor (at $x = 0$) were kept at levels not exceeding ± 5% and ± 3, respectively, from the reference values suggested by Sanmiguel Vila et al. [31]. It is also worth mentioning that the last profile in the measuring section (at $x = 1200$ mm) was relatively far from the separation point, which manifested as a relatively low value of the separation shape factor (2.6) introduced by Sandborn and Kline [73]. According to the authors, when this factor reached a value of 2.7 – 20% backflow is expected to occur, and such a value was reached at $x =$ 1250 mm in our experiment.

5. Effect of wavy wall parameters

As shown in the previous work [62], both the amplitude and period of waviness have a crucial impact on the potential enhancement of the skin friction throughout the amplitude modulation effect [66]. In Ref. [62], the maximum friction drag was achieved for $A/\lambda = 0.03$. However, this research was performed at a much lower Reynolds number ($Re_b = 6760$ based on the channel mean height and bulk velocity) than this study. Here, one may expect that the maximum skin friction will occur at different A/λ ratios. That is why, firstly, the effect of

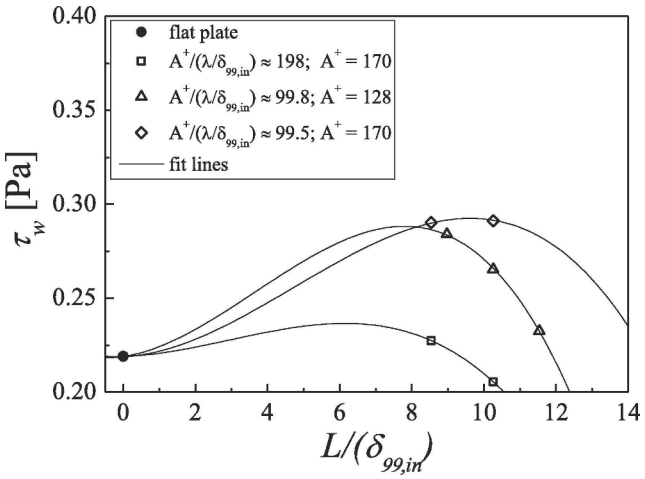

Fig. 6. Effect of the length of the wavy wall on the wall shear stress in the measuring section at $x = 1000$ mm.

the wave amplitude (for fixed $\lambda/\delta_{99,in} = 1.28$ and $L/\delta_{99,in} = 10.3$) on τ_w measured at $x = 1000$ is shown in Fig. 4 (see the open squares – cases 1–3 in Table 1). The filled circle corresponds to the reference case for which the skin friction was obtained for the flat plate. A third-order polynomial fit curve was used to estimate the position of the local maximum in τ_w. As can be seen, the wall shear stress first increases with increasing A^+ until reaching a local maximum for $A^+ \approx 170$, and then it starts to decrease. Such a maximum in τ_w corresponds to $A_{in}/\lambda = 0.033$, which is slightly higher than the one in Ref. [62] ($A/\lambda = 0.03$). Note, however, that for comparison, we used A_{in} (i.e. the amplitude of the first crest), as the amplitude of the wavy wall increased in the streamwise direction. Using another reference factor, for instance, the average amplitude, will give a much higher value of A/λ (note that the amplitude at the end of each wavy wall was about twice as high as A_{in}). An increase in A/λ is related to the much higher Reynolds number investigated in this study.

Fig. 5 presents the obtained values of wall shear stress in the measuring section at $x = 1000$ mm when separately changing the amplitude (marked as open squares) or the period (represented by open triangles). The filled circle corresponds to the reference case. Note, that the results presented in Fig. 5 were obtained under a fixed $L/\delta_{99,in} = 10.3$ and correspond to cases 1–5 in Table 1. As can be seen, there are three points, ensuring a growth in skin friction which are cases 1, 2, and 5 (Table 1). So, this may suggest that the amplitude assumed in case 3 was too high, and its optimal value exists somewhere between the amplitudes used in cases 1 and 2 (the first and the second square symbols from the left). Fig. 5 also indicates that a wider period λ may be more beneficial, as a substantial increase in skin friction was observed for case 5 (with 6 periods) up to $\tau_w = 0.299$ Pa relative to the one for the flat surface, where $\tau_w = 0.219$ Pa. For case 4 (with 12 total periods), a decrease in τ_w was recorded compared with the reference case.

Another important parameter that may have a substantial impact on skin friction control is the length of the wavy surface, which defines the limit of the pressure gradient for which the corrugation can be effectively applied. If the introduced corrugation is too short, the maximum enhancement of the skin friction will not be reached. If the corrugation is too long, it may also negatively influence momentum transfer from the outer to the inner region, as it may introduce a substantial drag and, hence, increase the volume occupied by the separation bubble. Fig. 6 demonstrates the effect of the wavy surface length on the skin friction. Note that the results are classified into three groups: first marked with squares (cases 4 and 6) with a medium amplitude $A^+ = 170$ and a small period $\lambda/\delta_{99,in} \approx 0.854$ (relative to the range of investigated parameters); second, marked with triangles (cases 1, 7, and 8) represent the small amplitude $A^+ \approx 128$ and the medium period $\lambda/\delta_{99,in} = 1.28$; third,

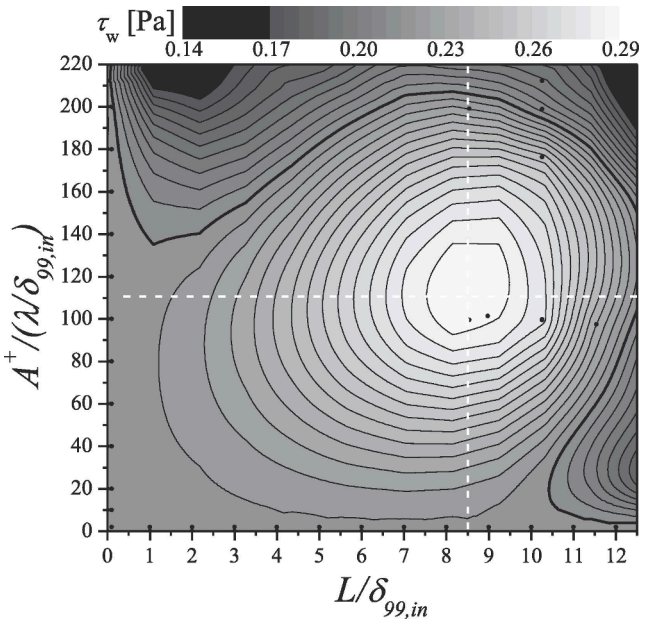

Fig. 7. The wall shear stress at $x = 1000$ mm as a function of normalised wave amplitude and length.

marked with diamonds (cases 5 and 9) represent the medium amplitude $A^+ = 170$ and the large period $\lambda/\delta_{99,in} = 1.71$. As can be seen from Fig. 6, the period used in the first group was too small, and only a small gain in skin friction was obtained for the shorter corrugation. Much better results were obtained when the cases from group 2 were used. Here, one may observe that the predicted local maximum in the skin friction should be located at $L/\delta_{99,in} \approx 8$ (see the line fitting triangles). The highest values of the skin friction (up to 0.299, which gives a 33.0% increase with respect to the reference case) were achieved when the wavy wall geometries from group 3 were used.

Finally, all obtained data were used to visualise the combined effect of all three waviness parameters by plotting τ_w as a function of dimensionless $A^+/(\lambda\ /\delta_{99,in})$ and $L/\delta_{99,in}$ at $x = 1000$ mm in Fig. 7. The measured values were plotted on an isocontour map and marked as black dots. Note that additional points were uniformly introduced on the boundaries along each axis with τ_w values corresponding to the reference case. Also, the second set of points located slightly away from each axis (which are visible in Fig. 7) with slightly higher skin friction values than those on the axes were included. Such a procedure ensured an asymptotic decrease in skin friction from its maximum value to the one on the flat plate. One may observe a local maximum at $A^+/(\lambda\ /\delta_{99,in}) \approx 110$, $\lambda\ /\delta_{99,in} = 1.71$, which corresponds to $A_{in}/\lambda = 0.028$, $L/\delta_{99,in} \approx 8.5$ and $\beta \approx 10$ (the last one is regarded as the upper approximate pressure gradient limit that determines the location that the waviness can reach). These results indicate that among the examined geometries, one may distinguish near-optimal corrugation parameters that provide a strong rise in wall shear stress.

6. Effect of the waviness downstream the flow.

The contour map in Fig. 7 allowed the determination of the most effective values of the examined wavy wall parameters. Fig. 8 demonstrates the effect of the most effective surface corrugation (case 9 from Table 1) on the distribution of δ_{99}, δ^* (which is the displacement thickness), H, β and τ_w parameters characterising TBL under APG conditions. The black symbols correspond to the reference case, while the red ones were obtained in the presence of a wavy wall (for case 9, which ensured the largest growth in τ_w at $x = 1000$ mm). As can be seen, the waviness is very beneficial as it causes a clear reduction in δ_{99}, δ^*, H, β and a huge growth in τ_w within the investigated streamwise distance from $x = 900$ mm to $x = 1200$ mm. It is also worth noting that the distributions slightly diverge downstream the flow, which is particularly evident in Fig. 6 c, d, and e. So, the relative difference in τ_w between the reference case and case 9 notably increases from 24% for $x = 900$ mm to 109% for $x = 1200$ mm. It is, however, interesting to estimate the relative growth in wall shear stress at the separation location on the flat plate. In this regard, we extrapolated the data from Fig. 8e downstream the flow. It can be observed that the most effective wavy wall geometry design (case 9) ensured 13% growth (up to $\tau_w = 0.095$ Pa) in the skin friction (relative to the inlet condition – $\tau_{w,ZPG} = 0.73$ Pa) at the location of the flow separation ($x = 1300$ mm – Fig. 8e) on the unmodified surface (i.e. on the flat plate). Moreover, the separation point shifted 150 mm downstream the channel.

In order to obtain a more detailed insight into how the flow was modified by the wavy wall, the profiles of mean velocity, Reynolds stress, skewness factor, and convection velocity are presented in the first, second, third, and fourth row, respectively, in Fig. 9. Note that the mean velocity, Reynolds stress, and mean convection velocity are normalised by the edge velocity U_e. In addition, the streamwise evolution, from $x = 900$ mm to $x = 1200$ mm, of these profiles is shown in subsequent columns. The black lines correspond to the flat plate case, whereas the red ones represent the profiles obtained when the surface waviness was used (for case 9 from Table 1), which ensured the largest growth in τ_w. Evidently, regardless of the distance x, all mean velocity profiles (obtained on the flat plate and those measured in the presence of wall undulations) collapse in the outer region, which means that modifications to the wall surface do not affect this region. In the inner part, a notable increase in mean velocity caused by the waviness is observed. This is directly related to a change in convection velocity, the distributions of which are shown in the last row of Fig. 9. A direct comparison between the Reynolds stress profiles indicates that the wavy surface is responsible for flattening and shifting the outer maximum. This is most likely the result of the effect of the wavy surface on LSM. Above $y/\delta = 0.6$, both profiles tend to collapse for each analysed distance x. One may also observe that the difference in the maximum Reynolds stress (in the outer region) increases with increasing x. The Reynolds stress distributions also indicate a growth in uu in the near-wall region, which is due to an increased strain rate induced by the amplitude modulation effect, as indicated by a lower skewness factor (which is even better visible in the spatial spectra in Fig. 10). The skewness factor profiles exhibit a shift of the zero-crossing location upward away from the wall, which is correlated with the shift of maximum in Reynolds stress profiles.

The convection velocity profiles, presented in the last row, were calculated using the distribution of the cross product term $\overline{3u_S^2 u_L}$ of decomposed skewness factor introduced in Ref. [53]. This approach was further verified using a two-point correlation as shown in Ref. [54]. As pointed out in Ref. [53], the net convection velocity substantially increases downstream in APG flow. Such an increase is directly related to the enhanced amplitude modulation (manifested by a greater difference in the momentum between high and low-speed regions), which alternates the production of turbulence. The wavy wall acts on TBL in a similar way as the low- and high-speed regions. Turbulence is generated mostly in high-speed regions and have increased streamwise convection with respect to the mean flow. An increased convection increases positive sweep events (which is manifested by increased skewness factor of the streamwise velocity with respect to ZPG flow) and in turn, increases the momentum transfer to the wall [53]. A similar observation was reported by Koyama et al. [61], but for the deformation of a wall boundary over time (i.e. using the active-flow control method). The result of this mechanism is a higher wall shear stress with respect to either the flow in the absence of an amplitude modulation effect, or to the flow affected by a wavy surface. Therefore, the new turbulence created locally under a higher momentum just behind the wavy wall induces lower sweep events and a lower skewness near the wall (compared with those at the flat plate). Even though the amplitude modulation becomes weaker

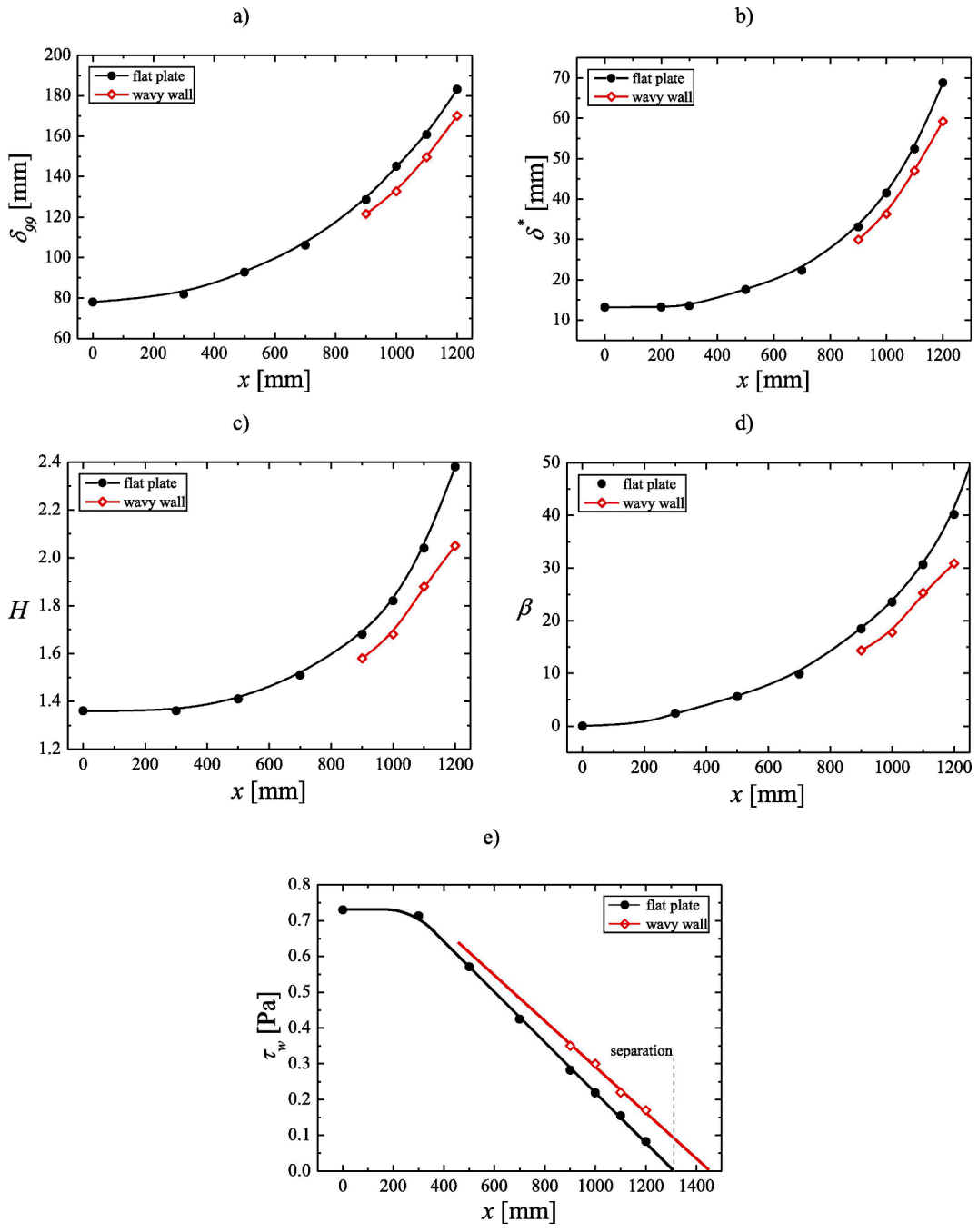

Fig. 8. Effect of the wavy wall on the streamwise distribution of δ_{99} (a), δ^*(b), H (c), β (d), and τ_w (e). wavy wall geometry corresponds to the case 9 from Table 1.

behind the wavy wall (which is manifested as a lower skewness), the convection velocity is still much higher than the flat-plate case. Hence, it seems that the skin friction enhancement mechanism is caused by increased convection velocity downstream of the corrugation, which reflects the changes of TBL parameters shown in Fig. 8. These results confirm the validity of the original mechanism related to an increased convection velocity due to amplitude modulation proposed by Dróżdż and Elsner [53].

As a complement to the presented results, the wavelet energy spectra E (equivalent to the premultiplied energy spectra) scaled by the edge velocity U_e are presented as a function of normalised streamwise length λ/δ and normalised wall distance y/δ in Fig. 10 at $x = 900$, 1000, 1100, and 1200 mm (Fig. 10 a, b, c, and d, respectively). The streamwise length λ was calculated based on the timescale through the Taylor hypothesis; however, due to the difference between the mean and convection velocities, U_c was used instead of U (shown in Fig. 9). The black isocontours correspond to the flat plate reference case, while the greyscale map refers to the wavy wall (case 9 from Table 1). Both share the same scale (i.e. the black lines represent the original shape and positions of certain levels of the greyscale isocontours). The maxima in each figure represent the contribution of LSM. Note, that the presence of the inner maxima in turbulence energy (which are characteristic of ZPG flows) are not visible here as they are hidden beneath the outer one (which is typical for high pressure gradient conditions) – see Ref. [67]. The location of the outer maximum, which represents the activity of LSM for the wavy wall case, shifted towards higher y/δ values due to flow interaction with waviness crests (due to increased wall-normal convection of large scales). After the wavy wall, the location of the maximum remained at approximately constant $y/\delta \approx 0.3$ in the pressure gradient. It is correlated with both the location of the outer maximum in the

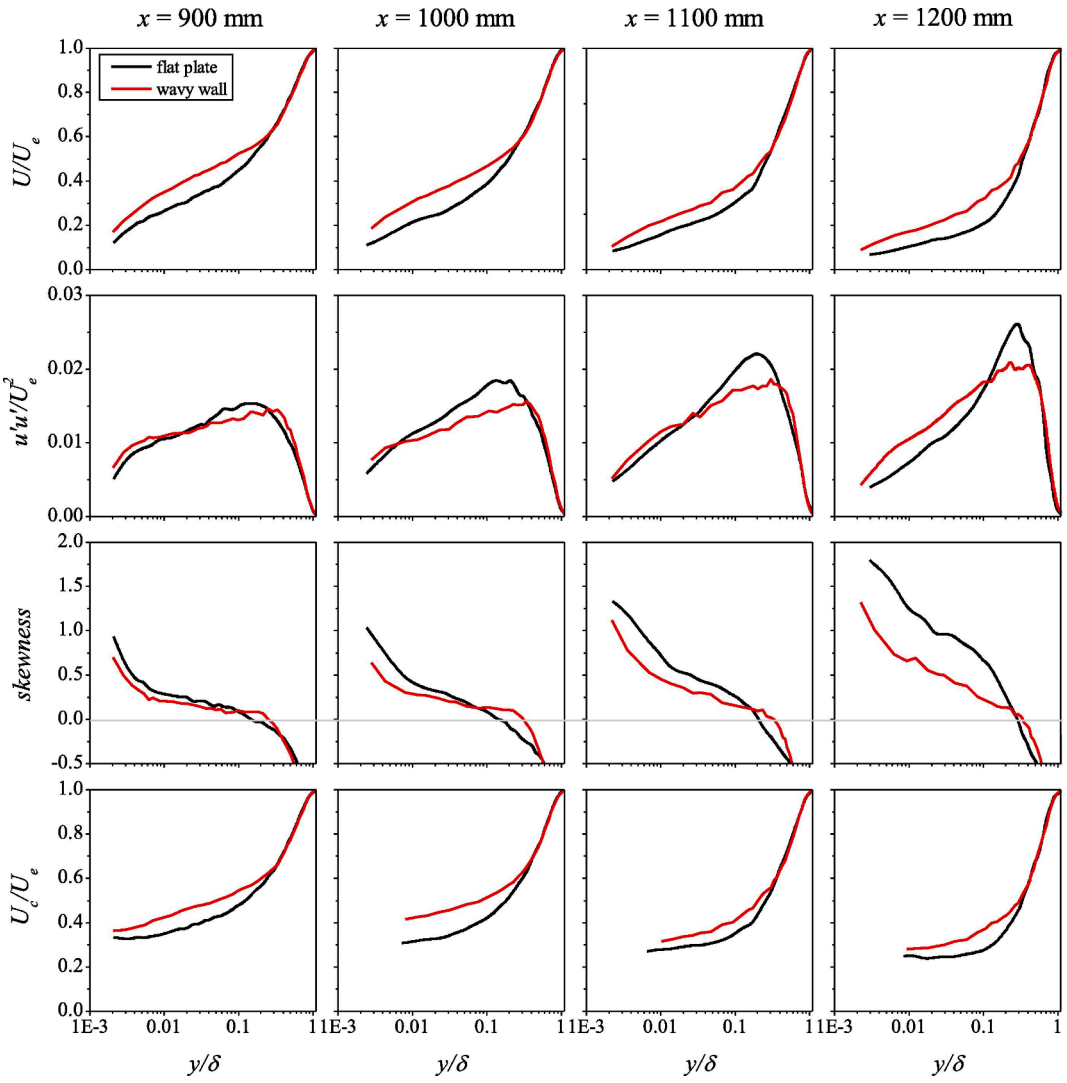

Fig. 9. Effect of a wavy surface on mean velocity, streamwise Reynolds stress, skewness factor and convection velocity profiles at $x = 900$, 1000, 1100 and 1200 mm (wavy wall profiles correspond to case 9 from Table 1).

streamwise Reynolds stress profiles and the location close to the zero-crossing skewness factor visible in Fig. 9, which was also previously showed in Ref. [69]. The outer spectral peak appears at $\lambda \approx 3\delta$, which is consistent with an earlier study by Harun et al. [45]; however, for the last two locations (Fig. 10 c and d), the dominant spatial scale shrinks to 2δ. It is also evident that in the near-separation region, there is a substantial reduction in the length scale of the maximum energy downstream of the flow (see the white dashed lines in Fig. 10). The most important conclusion of this observation of the spatial spectra is that the wavy wall causes an increased activity of the small-scales close to the wall (see the regions within $0 < y/\delta < 0.02$; $0 < \lambda/\delta < 1$, marked by white dotted lines), which manifested as higher energy values relative to the reference case. On the other hand, for the small scales above $y/\delta > 0.02$, there is less energy for the wavy wall. This effect is maintained at all investigated streamwise locations.

7. Conclusions

Recent experience in the use of various wall topologies and rough surfaces for sufficiently high Reynolds numbers in APG has revealed that such types of passive flow control methods cause earlier separation and enlarge the separation area. The discovery of the amplitude modulation process provided a better understanding of momentum transport from the outer to the inner part of the boundary layer and its effect on skin friction.

In this work, we demonstrated that it is possible to enhance the amplitude modulation effect using a wavy surface and, in turn, increase the skin friction and postpone separation. All the wavy wall cases investigated were designed to have a fixed wave amplitude in viscous units. The research mainly focussed on examining the effect of different amplitudes, periods, and lengths of wavy surfaces on increased wall shear stress. The analysis allowed the determination of the effective (which seems to be close to optimal for the given flow history conditions, APG strength, and Reynolds number) wavy wall geometry that ensures a 13% growth in skin friction (relative to the inlet condition) at the location of the flow separation on an unmodified surface (i.e. on the flat plate). The normalised dimensions of such a wavy wall were $A^+/(\lambda/\delta_{99,in}) \approx 110$, $\lambda/\delta_{99,in} = 1.71$ and $L/\delta_{99,in} \approx 8.5$. The last parameter simultaneously determines the upper limit of the wavy wall application in terms of the Clauser-Rotta pressure gradient parameter $\beta \approx 10$.

More detailed studies of the results showed that the waviness increases the mean velocity near the wall, but without a footprint in the outer region. The Reynolds stress distributions are also increased in the near-wall region. Such an effect is caused by an increased strain rate behind the wavy wall, which is manifested by lower skewness factor close to the wall. The outer maximum of the Reynolds stress profiles is

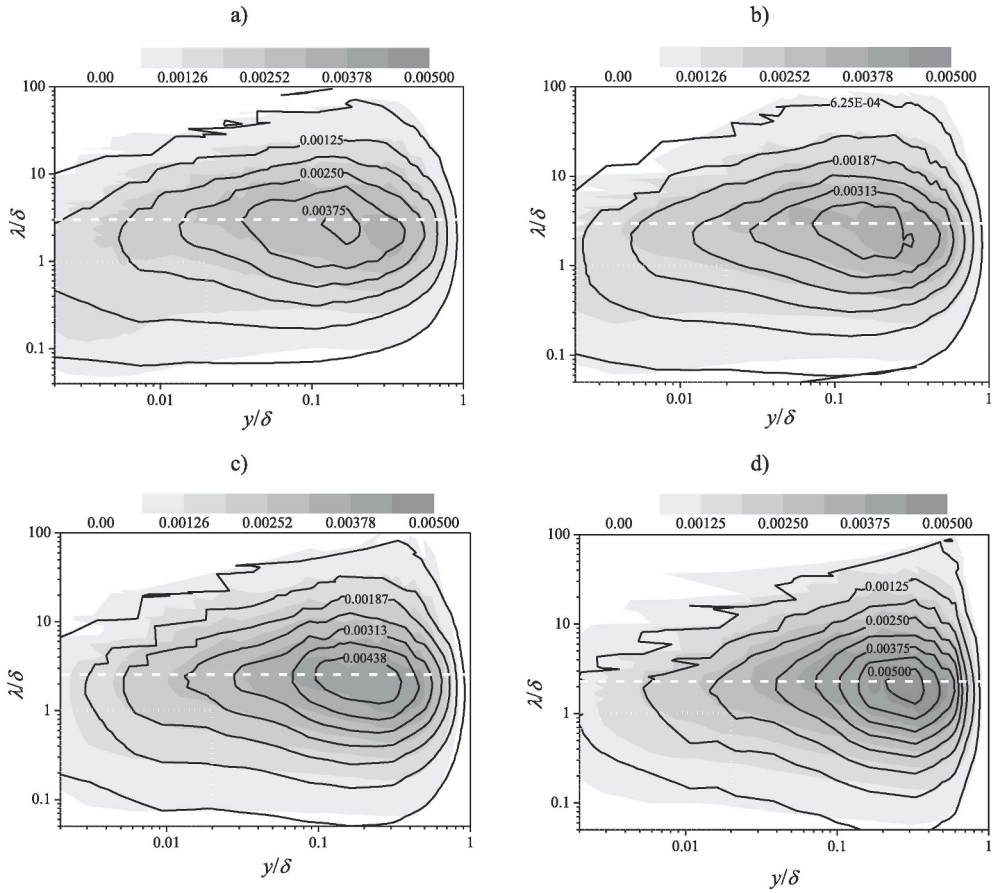

Fig. 10. Pre-multiplied energy spectra for $x = 900$ mm (a), $x = 1000$ mm (b), $x = 1100$ mm (c) and $x = 1200$ mm (d). Black isocontours correspond to the flat plate while the grey scale map represents the wavy wall case 9.

flattened and shifted upward away from the wall. The skewness factor profiles exhibit a shift of the zero-crossing location upward away from the wall, which is correlated with a shift of the maximum in Reynolds stress profiles.

The key finding was the increased convection velocity in the near-wall region using wall corrugation with specific parameters. The higher convection, the higher sweep events (which is manifested by an increased skewness factor of streamwise velocity), and in turn, the higher momentum transfer to the wall. Hence, one may conclude that the wavy wall acts on the TBL in a similar manner as the low and high-speed regions induced by LSM. Namely, the turbulence is generated mostly in high-speed regions and have increased convection with respect to the mean flow. Consequently, an increased wall shear stress with respect to the flat plate is observed.

Studies of the premultiplied energy spectra showed that the location of the outer maxima for both reference and wavy wall cases move towards higher y/δ values downstream of the flow. It is directly correlated with both the location of the outer maximum in the streamwise Reynolds stress profiles and the location close to the zero-crossing skewness factor.

Most importantly, observation of the spatial spectra of the wavy wall indicated increased activity of the small-scales close to the wall: for $y/\delta < 0.02$; $\lambda/\delta < 1$. However, above $y/\delta > 0.02$ the small-scales were found to be less energetic for the wavy wall case. This effect was maintained at all investigated streamwise locations, and it is related to a rise in the convection velocity and enhanced energy transfer to the wall.

Future research should focus on adopting the streamwise waviness on the surface of an airfoil behind the vortex generators to increase the friction drag and postpone separation. The research should be performed using a full-scale model and at a high Reynolds number. It is expected that the application of the proposed non-dimensional wavy surface parameters from the present study should increase the lift-to-drag ratio and substantially stabilise the flow on the suction side of the wing at a high angle of attack.

CRediT authorship contribution statement

Artur Dróżdż: Conceptualization, Methodology, Software, Investigation, Supervision, Formal analysis, Writing - review & editing. **Paweł Niegodajew:** Methodology, Investigation, Writing - original draft, Writing - review & editing. **Mathias Romańczyk:** Methodology, Investigation. **Vasyl Sokolenko:** Investigation. **Witold Elsner:** Funding acquisition, Project administration, Resources, Supervision, Methodology, Writing - review & editing.

Declaration of Competing Interest

The authors declare that they have no known competing financial interests or personal relationships that could have appeared to influence the work reported in this paper.

Acknowledgement

The investigation was supported by National Science Centre under Grant No. DEC-2017/25/B/ST8/02480.

Appendix A

The corrected Clauser-chart method (CCCM) presented by Niegodajew et al. [69] was found to ensure a very good estimation of the

Table 2
Verification of CCCM against oil-film interferometry measurements.

A/λ	u_τ [m/s] (OFI) [66]	u_τ [m/s] (CCCM)	Error [%]
0.025	0.431	0.432	0.15
0.04	0.456	0.460	0.96
0.06	0.488	0.482	−1.27
0.08	0.494	0.486	−1.59

friction velocity under APG flows up to $\beta = 28$. In the present study, the flow in the APG section was also modified by the wall undulation and so, one may find it questionable whether the method is valid in such a configuration. Our previous work [66] includes oil-film interferometry measurements performed in APG behind the wavy wall and for four different A/λ configurations from 0.025 to 0.08 and a similar range of A^+ as in the present study. Hence, herein we used this data to verify the validity of CCCM in the region behind the waviness, and the results in the form of friction velocity $u_\tau = (\tau_w/\rho)$ measured using OFI and estimated with CCCM are presented in Table 2. As can be seen, the uncertainty of CCCM do not exceed 1.6% for the available wavy wall configurations, which confirms the validity of the method.

References

[1] M. Gad-el-Hak, D.M. Bushnell, Separation control: review, J. Fluids Eng. 113 (1991) 5–30.
[2] C.M. White, M.G. Mungal, Mechanics and prediction of turbulent drag reduction with polymer additives, Annu. Rev. Fluid Mech. 40 (2008) 235–256, https://doi.org/10.1146/annurev.fluid.40.111406.102156.
[3] X. Zhang, X. Duan, Y. Muzychka, Degradation of flow drag reduction with polymer additives — a new molecular view, J. Mol. Liq. 292 (2019) 111360, https://doi.org/10.1016/j.molliq.2019.111360.
[4] S.A. Mäkiharju, S.L. Ceccio, On multi-point gas injection to form an air layer for frictional drag reduction, Ocean Eng. 147 (2018) 206–214, https://doi.org/10.1016/j.oceaneng.2017.10.041.
[5] X. Zhao, Z. Zong, Y. Jiang, T. Sun, A numerical investigation of the mechanism of air-injection drag reduction, Appl. Ocean Res. 94 (2020) 101978, https://doi.org/10.1016/j.apor.2019.101978.
[6] M. Atzori, R. Vinuesa, G. Fahland, A. Stroh, D. Gatti, B. Frohnapfel, P. Schlatter, Aerodynamic effects of uniform blowing and suction on a NACA4412 airfoil, flow, Turbul. Combust. (2020), https://doi.org/10.1007/s10494-020-00135-z.
[7] H.S. Yoon, O.A. El-Samni, H.H. Chun, Drag reduction in turbulent channel flow with periodically arrayed heating and cooling strips, Phys. Fluids 18 (2006) 025104, https://doi.org/10.1063/1.2171196.
[8] M. Kotenko, H. Oskarsson, C. Bojesen, M.P. Nielsen, An experimental study of the drag reducing surfactant for district heating and cooling, Energy. 178 (2019) 72–78, https://doi.org/10.1016/j.energy.2019.03.134.
[9] M. Quadrio, Drag reduction in turbulent boundary layers by in-plane wall motion, Philos. Trans. R. Soc. A Math. Phys. Eng. Sci. 369 (2011) 1428–1442, https://doi.org/10.1098/rsta.2010.0366.
[10] N. Tomiyama, K. Fukagata, Direct numerical simulation of drag reduction in a turbulent channel flow using spanwise traveling wave-like wall deformation, Phys. Fluids 25 (2013), https://doi.org/10.1063/1.4826887.
[11] V. Shatrov, G. Gerbeth, Magnetohydrodynamic drag reduction and its efficiency, Phys. Fluids 19 (2007), https://doi.org/10.1063/1.2714077.
[12] H.O.G. Benschop, W.P. Breugem, Drag reduction by herringbone riblet texture in direct numerical simulations of turbulent channel flow, Phys. Fluids. (2017). http://arxiv.org/abs/1703.10879.
[13] F. Afroz, A. Lang, M.L. Habegger, P. Motta, R. Hueter, Experimental study of laminar and turbulent boundary layer separation control of shark skin, Bioinspiration Biomimetics 12 (2017) 016009, https://doi.org/10.1088/1748-3190/12/1/016009.
[14] A.W. Lang, E.M. Jones, F. Afroz, Separation control over a grooved surface inspired by dolphin skin, Bioinspiration Biomimetics 12 (2017), https://doi.org/10.1088/1748-3190/aa5770.
[15] Y. Luo, L. Wang, L. Green, K. Song, L. Wang, R. Smith, Advances of drag-reducing surface technologies in turbulence based on boundary layer control, J. Hydrodyn. 27 (2015) 473–487, https://doi.org/10.1016/S1001-6058(15)60507-8.
[16] F.H. Clauser, The turbulent boundary layer, Adv. Appl. Mech. 4 (1956) 1–51, https://doi.org/10.1016/S0065-2156(08)70370-3.
[17] M.R. Raupach, R.A. Antonia, S. Rajagopalan, Rough-wall turbulent boundary layers, Appl. Mech. Rev. 44 (1991).
[18] J. Yuan, U. Piomelli, Roughness effects on the Reynolds stress budgets in near-wall turbulence, J. Fluid Mech. 760 (2014) R1, https://doi.org/10.1017/jfm.2014.608.
[19] T.O. Jelly, A. Busse, Reynolds number dependence of Reynolds and dispersive stresses in turbulent channel flow past irregular near-Gaussian roughness, Int. J. Heat Fluid Flow 80 (2019) 108485, https://doi.org/10.1016/j.ijheatfluidflow.2019.108485.
[20] S. Hansda, K. Barman, S. Roy, K. Debnath, Quantification of turbulent eddies in time-space and frequency domain for wave-current combined flow over side-wall roughness, Ocean Eng. 186 (2019) 106080, https://doi.org/10.1016/j.oceaneng.2019.05.062.
[21] S. Song, J. Eaton, The effects of wall roughness on the separated flow over a smoothly contoured ramp, Exp. Fluids 33 (2002) 38–46, https://doi.org/10.1007/s00348-002-0411-1.
[22] C.D. Aubertine, J.K. Eaton, S. Song, Parameters controlling roughness effects in a separating boundary layer, Int. J. Heat Fluid Flow 25 (2004) 444–450, https://doi.org/10.1016/j.ijheatfluidflow.2004.02.007.
[23] W. Wu, U. Piomelli, Effects of surface roughness on a separating turbulent boundary layer, J. Fluid Mech. 841 (2018) 552–580, https://doi.org/10.1017/jfm.2018.101.
[24] J.M. Tsikata, M.F. Tachie, Adverse pressure gradient turbulent flows over rough walls, Int. J. Heat Fluid Flow 39 (2013) 127–145, https://doi.org/10.1016/j.ijheatfluidflow.2012.11.001.
[25] J.M. Tsikata, M.F. Tachie, Effects of roughness and adverse pressure gradient on the turbulence structure, Int. J. Heat Fluid Flow 44 (2013) 239–257, https://doi.org/10.1016/j.ijheatfluidflow.2013.06.003.
[26] J.H. Lee, Turbulent boundary layer flow with a step change from smooth to rough surface, Int. J. Heat Fluid Flow 54 (2015) 39–54, https://doi.org/10.1016/j.ijheatfluidflow.2015.05.001.
[27] R. Wahidi, W. Chakroun, S. Al-Fahed, The behavior of the skin-friction coefficient of a turbulent boundary layer flow over a flat plate with differently configured transverse square grooves, Exp. Therm Fluid Sci. 30 (2005) 141–152, https://doi.org/10.1016/j.expthermflusci.2005.03.022.
[28] M. Sasamori, H. Mamori, K. Iwamoto, A. Murata, Experimental study on drag-reduction effect due to sinusoidal riblets in turbulent channel flow, Exp. Fluids 55 (2014), https://doi.org/10.1007/s00348-014-1828-z.
[29] H. Mamori, K. Yamaguchi, M. Sasamori, K. Iwamoto, A. Murata, Dual-plane stereoscopic PIV measurement of vortical structure in turbulent channel flow on sinusoidal riblet surface, Eur. J. Mech. – B/Fluids. 74 (2019) 99–110, https://doi.org/10.1016/j.euromechflu.2018.11.006.
[30] P. Schlatter, R. Örlü, Turbulent boundary layers at moderate Reynolds numbers: Inflow length and tripping effects, J. Fluid Mech. 710 (2012) 5–34, https://doi.org/10.1017/jfm.2012.324.
[31] C. Sanmiguel Vila, R. Vinuesa, S. Discetti, A. Ianiro, P. Schlatter, R. Örlü, On the identification of well-behaved turbulent boundary layers, J. Fluid Mech. 822 (2017) 109–138, https://doi.org/10.1017/jfm.2017.258.
[32] E. Rodríguez-López, P.J.K. Bruce, O.R.H. Buxton, On the formation mechanisms of artificially generated high reynolds number turbulent boundary layers, Boundary-Layer Meteorol. 160 (2016) 201–224, https://doi.org/10.1007/s10546-016-0139-8.
[33] J.H. McMasters, M.L. Henderson, Low-speed single-element airfoil synthesis, Technical Soar. 6 (1979) 1689–1699, https://doi.org/10.1017/CBO9781107415324.004.
[34] D. Luo, D. Huang, X. Sun, Passive flow control of a stalled airfoil using a microcylinder, J. Wind Eng. Ind. Aerodyn. 170 (2017) 256–273, https://doi.org/10.1016/j.jweia.2017.08.020.
[35] Y. Wang, G. Li, S. Shen, D. Huang, Z. Zheng, Investigation on aerodynamic performance of horizontal axis wind turbine by setting micro-cylinder in front of the blade leading edge, Energy. 143 (2018) 1107–1124, https://doi.org/10.1016/j.energy.2017.10.094.
[36] R. Belamadi, A. Djemili, A. Ilinca, R. Mdouki, Aerodynamic performance analysis of slotted airfoils for application to wind turbine blades, J. Wind Eng. Ind. Aerodyn. 151 (2016) 79–99, https://doi.org/10.1016/j.jweia.2016.01.011.
[37] S. Beyhaghi, R.S. Amano, A parametric study on leading-edge slots used on wind turbine airfoils at various angles of attack, J. Wind Eng. Ind. Aerodyn. 175 (2018) 43–52, https://doi.org/10.1016/j.jweia.2018.01.007.
[38] J.J. Wang, Y.C. Li, K.S. Choi, Gurney flap-Lift enhancement, mechanisms and applications, Prog. Aerosp. Sci. 44 (2008) 22–47, https://doi.org/10.1016/j.paerosci.2007.10.001.
[39] Z. Wang, M. Zhuang, Leading-edge serrations for performance improvement on a vertical-axis wind turbine at low tip-speed-ratios, Appl. Energy 208 (2017) 1184–1197, https://doi.org/10.1016/j.apenergy.2017.09.034.
[40] L. Zhang, X. Li, K. Yang, D. Xue, Effects of vortex generators on aerodynamic performance of thick wind turbine airfoils, J. Wind Eng. Ind. Aerodyn. 156 (2016) 84–92, https://doi.org/10.1016/j.jweia.2016.07.013.
[41] H. Zhu, W. Hao, C. Li, Q. Ding, B. Wu, A critical study on passive flow control techniques for straight-bladed vertical axis wind turbine, Energy 165 (2018) 12–25, https://doi.org/10.1016/j.energy.2018.09.072.
[42] N. Hutchins, I. Marusic, Evidence of very long meandering features in the logarithmic region of turbulent boundary layers, J. Fluid Mech. 579 (2007) 1–28, https://doi.org/10.1017/S0022112006003946.
[43] N. Hutchins, I. Marusic, Large-scale influences in near-wall turbulence, Philos. Trans. R. Soc. A Math. Phys. Eng. Sci. 365 (2007) 647–664, https://doi.org/10.1098/rsta.2006.1942.
[44] R. Mathis, N. Hutchins, I. Marusic, Large-scale amplitude modulation of the small-scale structures in turbulent boundary layers, J. Fluid Mech. 628 (2009) 311–337, https://doi.org/10.1017/S0022112009006946.
[45] Z. Harun, J.P. Monty, R. Mathis, I. Marusic, Pressure gradient effects on the large-scale structure of turbulent boundary layers, J. Fluid Mech. 715 (2013) 477–498, https://doi.org/10.1017/jfm.2012.531.
[46] M. Nadeem, J.H. Lee, J. Lee, H.J. Sung, Turbulent boundary layers over sparsely-spaced rod-roughened walls, Int. J. Heat Fluid Flow 56 (2015) 16–27, https://doi.org/10.1016/j.ijheatfluidflow.2015.06.006.

[47] J. Basley, L. Perret, R. Mathis, Spatial modulations of kinetic energy in the roughness sublayer, J. Fluid Mech. 850 (2018) 584–610, https://doi.org/10.1017/jfm.2018.458.
[48] G. Pathikonda, K.T. Christensen, Inner-outer interactions in a turbulent boundary layer overlying complex roughness, Phys. Rev. Fluids 2 (2017), https://doi.org/10.1103/PhysRevFluids.2.044603.
[49] W. Anderson, Amplitude modulation of streamwise velocity fluctuations in the roughness sublayer: evidence from large-eddy simulations, J. Fluid Mech. 789 (2016) 567–588, https://doi.org/10.1017/jfm.2015.744.
[50] W.J. Baars, N. Hutchins, I. Marusic, Reynolds-number trend of hierarchies and scale interactions in turbulent boundary layers, Philos. Trans. R. Soc. London. Ser. A Math. Phys. Sci. 375 (2017) 18.
[51] C. Zhang, S.I. Chernyshenko, Quasisteady quasihomogeneous description of the scale interactions in near-wall turbulence, Phys. Rev. Fluids 1 (2016) 014401, https://doi.org/10.1103/PhysRevFluids.1.014401.
[52] A. Dróżdż, Influence of pressure gradient on streamwise skewness factor in turbulent boundary layer, J. Phys. Conf. Ser. 530 (2014) 012061, https://doi.org/10.1088/1742-6596/530/1/012061.
[53] A. Dróżdż, W. Elsner, Amplitude modulation and its relation to streamwise convection velocity, Int. J. Heat Fluid Flow 63 (2017) 67–74, https://doi.org/10.1016/j.ijheatfluidflow.2016.11.013.
[54] A. Dróżdż, W. Elsner, Convection velocity variation as a result of amplitude modulation phenomena, in: P.J. Örlü R., Talamelli A., Oberlack M. (Ed.), Prog. Turbul. VII, Springer Proceedings in Physics, vol. 196. Springer, Cham, 2017, pp. 33–38. https://doi.org/10.1007/978-3-319-57934-4_5.
[55] L. Agostini, M. Leschziner, The connection between the spectrum of turbulent scales and the skin-friction statistics in channel flow at Re $\tau \approx 1000$, J. Fluid Mech. 871 (2019) 22–51, https://doi.org/10.1017/jfm.2019.297.
[56] N. Kruse, S. Kuhn, P.R. Von Rohr, Wavy wall effects on turbulence production and large-scale modes, J. Turbul. 7 (2006) 1–24, https://doi.org/10.1080/14685240600602911.
[57] S. Ganju, J. Davis, S.C.C. Bailey, C. Brehm, Direct numerical simulations of turbulent channel flows with sinusoidal walls, in: AIAA SciTech Forum 7-11 January 2019, San Diego, Calif., 2019. https://doi.org/10.2514/6.2019-2141.
[58] V.C. Patel, J. Tyndall Chon, J.Y. Yoon, Turbulent flow in a channel with a wavy wall, J. Fluids Eng. Trans. ASME 113 (1991) 579–586, https://doi.org/10.1115/1.2926518.
[59] H. Fujii, Turbulence Structure, Friction Drag and Pressure Drag Due To Turbulent Flow Over Angled Wavy Surfaces, 2009.
[60] S. Ghebali, S.I. Chernyshenko, M.A. Leschziner, Turbulent skin-friction reduction by wavy surfaces, Phys. Fluids 29 (2017) 105102. http://arxiv.org/abs/1705.01989.
[61] S. Koyama, K. Takashima, Y. Hagiwara, Turbulence modification in flow around a periodically deforming film, J. Turbul. 8 (2007), https://doi.org/10.1080/14685240701326808.
[62] H.S. Yoon, O.A. El-Samni, A.T. Huynh, H.H. Chun, H.J. Kim, A.H. Pham, I.R. Park, Effect of wave amplitude on turbulent flow in a wavy channel by direct numerical simulation, Ocean Eng. 36 (2009) 697–707, https://doi.org/10.1016/j.oceaneng.2009.03.012.
[63] S. Khan, B. Jayaraman, Statistical structure and deviations from equilibrium in wavy channel turbulence, Fluids 4 (2019), https://doi.org/10.3390/fluids4030161.
[64] V.M. Segunda, S.J. Ormiston, M.F. Tachie, Experimental and numerical investigation of developing turbulent flow over a wavy wall in a horizontal channel, Eur. J. Mech./B Fluids 68 (2018) 128–143, https://doi.org/10.1016/j.euromechflu.2017.12.001.
[65] A.M. Hamed, L. Castillo, L.P. Chamorro, Turbulent boundary layer response to large-scale wavy topographies, Phys. Fluids 29 (2017), https://doi.org/10.1063/1.4989719.
[66] A. Dróżdż, W. Elsner, D. Sikorski, Passive skin friction control near turbulent separation – preliminary results, J. Phys. Conf. Ser. 1101 (2018) 012004.
[67] A. Dróżdż, W. Elsner, An experimental study of turbulent boundary layers approaching separation, Int. J. Heat Fluid Flow 68 (2017) 337–347, https://doi.org/10.1016/j.ijheatfluidflow.2017.10.003.
[68] P.M. Ligrani, P. Bradshaw, Spatial resolution and measurement of turbulence in the viscous sublayer using subminiature hot-wire probes, Exp. Fluids 5 (1987) 407–417.
[69] P. Niegodajew, A. Dróżdż, W. Elsner, A new approach for estimation of the skin friction in turbulent boundary layer under the adverse pressure gradient conditions, Int. J. Heat Fluid Flow 79 (2019) 108456, https://doi.org/10.1016/j.ijheatfluidflow.2019.108456.
[70] M.H. Buschmann, M. Gad-el-hak, Recent developments in scaling of wall-bounded flows, Prog. Aerosp. Sci. 42 (2007) 419–467.
[71] M. Samie, I. Marusic, N. Hutchins, M.K. Fu, Y. Fan, M. Hultmark, A.J. Smits, Fully resolved measurements of turbulent boundary layer flows up to Re 20000, J. Fluid Mech. 851 (2018) 391–415, https://doi.org/10.1017/jfm.2018.508.
[72] Y. Ikeya, R. Örlü, K. Fukagata, P.H. Alfredsson, Towards a theoretical model of heat transfer for hot-wire anemometry close to solid walls, Int. J. Heat Fluid Flow 68 (2017) 248–256, https://doi.org/10.1016/j.ijheatfluidflow.2017.09.002.
[73] V.A. Sandborn, S.J. Kline, Flow models in boundary-layer stall inception, J. Basic Eng. 83 (1961) 317–327.